OPEN ACCESS
Saudi Journal of Engineering and Technology
Abbreviated Key Title: Saudi J Eng Technol
ISSN 2415-6272 (Print) |ISSN 2415-6264 (Online)
Scholars Middle East Publishers, Dubai, United Arab Emirates
Journal homepage: https://saudijournals.com

Original Research Article

Transverse Magnetic Field Effect on Extracellular Fluid Flow along with a Semi-Infinite Vertical Rotating Porous Plate

Avijit Podder[1], Md. Tusher Mollah[2], Mohammad Wahiduzzaman[1, 3], Giulio Lorenzini[4], Md. Mahmud Alam[1*]

[1]Mathematics Discipline, Science, Engineering and Technology School, Khulna University, Khulna-9208, Bangladesh
[2]Department of Mathematics, European University of Bangladesh, Dhaka 1216, Bangladesh
[3]Department of Mathematics, University of Rajshahi, Rajshahi-6205, Bangladesh
[4]Department of Engineering and Architecture, University of Parma, Parco Area delle Scienze 181/A, Parma 43124, Italy

DOI: 10.36348/sjet.2022.v07i05.003 | **Received:** 29.04.2022 | **Accepted:** 06.06.2022 | **Published:** 17.06.2022

***Corresponding author:** Md. Mahmud Alam
Mathematics Discipline, Science, Engineering and Technology School, Khulna University, Khulna-9208, Bangladesh

Abstract

The primary intention of this practice is to numerically investigate the extracellular fluid (ECF) flow for unsteady 2-dimenstional case along with a porous vertical plate with the appearance of a transverse magnetic field in a rotating system. The dimensional basic equations have been non-dimensionalized by necessary dimensionless variables. The EFDM has been practiced to solve the dimensionless equations. The numerical data have been evaluated by FORTRAN software version 6.6a. For a perfect conductivity, Magnetic Diffusivity Number values have been taken between 5 to 15 in the induction formula. For proper exactness, stability and convergence tests have been performed. For initial time $\tau = 1$, the outputs have been illustrated for the primary, secondary and angular velocity, primary and secondary induced magnetic field, temperature field with shear stresses for X and Z -direction, couple stress for Z -direction, X and Z -direction current densities and Nusselt number. Finally, the outcomes of different parameters are discussed separately and pictorial graphically by MATLAB R2018a.The findings of this research may be used to control cell temperature, measurement of extracellular fluid motion, and so on.

Keywords: Perfect Conducting Fluid, Rotating System, Finite Difference Numerical Method, Induced Magnetic Field, Rotation, Transverse Magnetic Field.

1. INTRODUCTION

Extracellular fluids are micro structural fluids with perfectly conductivity that demonstrate the outcomes and inertia of micro-rotation. Various series of biophysics have evolved from physiology. ECF has a big intentness of sodium cations (Na^{+}), with a low percentage of potassium cations (K^{+}) exterior the neuron structural and functional unit, and a big intentness of chloride anions (Cl^{-}) as well as a low percentage of potassium cations (K^{+}) inner side [1].

Hodgkin *et al.*, [2] investigated stimulation of a cell by a corporal outcome causes a nerve stimulation. Involving nerve cell activity.

Firstly, Eringen established the micropolar fluids theory that show the outcome of local inertia with rotating system involving couple stress [3]. Attractive results of the blood rheology connection have been evaluated by Kline-Alien [4]. Micropolar fluid for low density has been investigated by researchers as followed in Ariman [5]. Ariman *et al.*, also oversaw the micro-continuum fluid dynamics [6]. Eringen elaborated the theory of micropolar fluid and established the basic of thermo-micropolar fluids [7].

Ezzat *et al.*, found a research of a extracellular magneto-hydrodynamics boundary level flow [8]. Also, Ezzat established a farther ordinary base of MHD free convection flow including the heat conduction relaxation time with the electric displacement current [9]. Bhargava *et al.*, established the numerical output of magnetohydrodynamics free convection of the micropolar fluid flow between two vertical porous parallel plates [10]. Mohammadein et al. established a base to display the outputs in a micropolar fluid with of the transverse magnetic field [11]. Effects of magnetic fields were investigated by Postelnicu [12]. A micropolar boundary layer principle has been placed by Peddiesen with other researcher [13]. The impact of currents on free flowing current along a perforated boundary covered by a infinite vertical plate has been investigated by Ram [14]. The effect combination of thermal radiation with Hall current on moving a vertically perforated plate with rotation have been formulated by Garg [15]. Boundary layer heat-expansion and expansion-thermo flows with Soret and Dufour effects have been analyzed for mix convection by Kafoussias-Williams [16]. Hall current effect on MHD flow over a perpendicular surface in alveolar media by mixed convection has been generated by Shateyi *et al.*, [17]. Numerical solutions of MHD mixed convective flows including chemical heat generation reactions have been performed by Ahmed *et al.*, [18]. Hall current effect on MHD rotating flow for a moving plate with a magnetic field has been illustrated by Takhar *et al.*, [19]. Through all of these research papers, it is not found conception of the extracellular fluid flow with Hall and heat generation effects.

To solve these problems, this paper establishes a model by extending the work of Ezzat [1] with Hall current and rotating system for unsteady two-dimensional cases along with the porous vertical plate. Using dimensionless variables, the elementary main equations of the model have been non-dimensionalized. The gained dimensionless equations solved numerically by conducting the explicit finite difference formula. Stability and convergence test has been performed to obtain the proper solution. Finally, all feasible results have been expounded.

The leftover of this work is embodied as follows: Section 2 draws up the mathematical equations of the model, Section 3 describes the shear stresses, couple stress, current densities, and Nusselt number effects, Section 4 provides the numerical techniques with stability analysis, Section 5 indicates the outputs and discussion, and finally, Section 6 summarizes the conclusion which gives the final outcome of this model.

2. MATHEMATICAL FORMULATION

An unsteady ECF flow through a semi-infinite perpendicular porous plate with the transverse magnetic field, joule heating and viscous dissipation effect involving rotating system are considered. The direction of fluid motion is denoted as the positive x coordinate along with the plate and the y coordinate is denoted normal to the plate. Initially, it is taken into account that the plate as well as is at the same temperature $T\left(>T_\infty\right)$. Also, it is taken that the plate and the fluid is at rest and after that the plate is to be moving with a fixed velocity U_∞ in its own plate. Instantaneously at time $t>0$, the temperature of the plate raised to $T_w\left(>T_\infty\right)$, where T_w is the wall temperature and T_∞ is the temperature that is outside the plate, and the system is rotating anticlockwise where rotational velocity Ω. The physical configuration is illustrated in Figure 1.

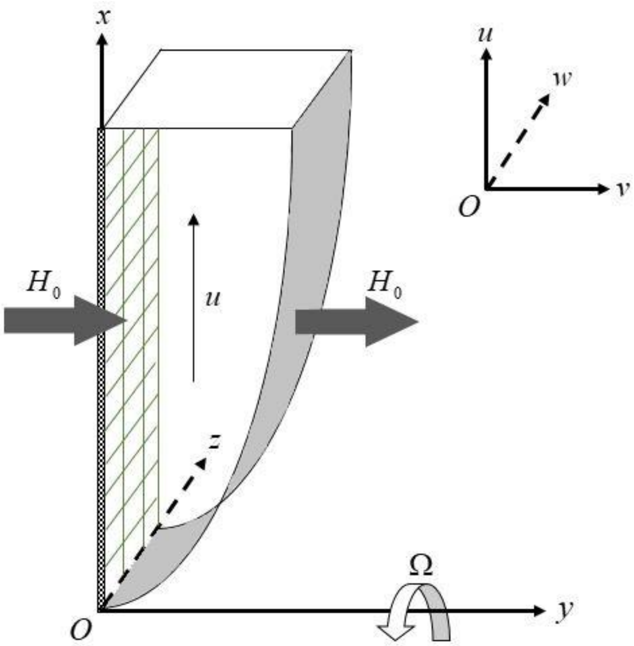

Figure 1: The physical configuration and coordinate system

A strong identical magnetic field H_0 has been accepted as $\left(0,H_0,0\right)$. For extracellular fluid, magnetic Reynolds number $R_m >> 1$ which gives the dimensionless Magnetic Diffusivity Number $\left(P_m\right)$

values from 5 to 15. The well known divergence equation $\nabla \cdot \mathbf{H} = 0$ of Maxwell's equation for the transverse magnetic field provides $H_y = H_0$. Using the formula $\nabla \cdot \mathbf{J} = 0$ for the current density vector $\mathbf{J} = (J_x, J_y, J_z)$ implies $J_y = \text{constant}$. As the porous plate is non-conducting, $J_y = 0$ at the plate and zero everywhere. The velocity vector of the fluid is taken by $\mathbf{q} = (u, v, w)$.

The used dimensionless variables as,

$$\tau = \frac{tU_\infty^{\ 2}}{\upsilon},\ U = \frac{u}{U_\infty},\ V = \frac{v}{U_\infty},\ W = \frac{w}{U_\infty},\ X = \frac{xU_\infty}{\upsilon},\ Y = \frac{yU_\infty}{\upsilon},\ N = \frac{\upsilon N_z}{U_\infty^{\ 2}},\ H_1 = \sqrt{\frac{\mu_e}{\rho}}\frac{H_x}{U_\infty},$$

$$H_3 = \sqrt{\frac{\mu_e}{\rho}}\frac{H_z}{U_\infty} \text{ and } \theta = \frac{T - T_\infty}{T_w - T_\infty}.$$

With the help of dimensionless variables, the main equations becomes,

$$\frac{\partial U}{\partial X} + \frac{\partial V}{\partial Y} = 0 \tag{1}$$

$$\frac{\partial U}{\partial \tau} + U\frac{\partial U}{\partial X} + V\frac{\partial U}{\partial Y} = G_r\theta + (1+\Delta)\frac{\partial^2 U}{\partial Y^2} + \Delta\frac{\partial N}{\partial Y} + M\frac{\partial H_1}{\partial Y} - \frac{U}{D_a} - RW \tag{2}$$

$$\frac{\partial W}{\partial \tau} + U\frac{\partial W}{\partial X} + V\frac{\partial W}{\partial Y} = (1+\Delta)\frac{\partial^2 W}{\partial Y^2} + M\frac{\partial H_3}{\partial Y} - \frac{W}{D_a} + RU \tag{3}$$

$$\frac{\partial N}{\partial \tau} + U\frac{\partial N}{\partial X} + V\frac{\partial N}{\partial Y} = \Lambda\frac{\partial^2 N}{\partial Y^2} - \lambda\frac{\partial U}{\partial Y} - 2\lambda N \tag{4}$$

$$\frac{\partial H_1}{\partial \tau} + V\frac{\partial H_1}{\partial Y} = \frac{1}{P_m}\frac{\partial^2 H_1}{\partial Y^2} + H_1\frac{\partial U}{\partial X} + M\frac{\partial U}{\partial Y} - \frac{\beta_e}{P_m}\frac{\partial^2 H_3}{\partial Y^2} \tag{5}$$

$$\frac{\partial H_3}{\partial \tau} + V\frac{\partial H_3}{\partial Y} = \frac{1}{P_m}\frac{\partial^2 H_3}{\partial Y^2} + H_1\frac{\partial W}{\partial X} + M\frac{\partial W}{\partial Y} + \frac{\beta_e}{P_m}\frac{\partial^2 H_1}{\partial Y^2} \tag{6}$$

$$\frac{\partial \theta}{\partial \tau} + U\frac{\partial \theta}{\partial X} + V\frac{\partial \theta}{\partial Y} = \frac{1}{P_r}\frac{\partial^2 \theta}{\partial Y^2} + \frac{E_c}{P_m}\left\{\left(\frac{\partial H_3}{\partial Y}\right)^2 + \left(\frac{\partial H_1}{\partial Y}\right)^2\right\} + E_c\left\{\left(\frac{\partial U}{\partial Y}\right)^2 + \left(\frac{\partial W}{\partial Y}\right)^2\right\} + \beta\theta^p \tag{7}$$

Resultant dimensionless boundaries,

$$U = 1,\ V = 0,\ W = 0,\ N = -S\frac{\partial U}{\partial Y},\ H_1 = \sqrt{\frac{\mu_e}{\rho}}\frac{H_w}{U_\infty} = 1(\text{say}),\ H_3 = 0,\ \theta = 1 \text{ at } Y = 0$$

$$U = 0,\ V = 0,\ W = 0,\ N = 0,\ H_1 = 0,\ H_3 = 0,\ \theta \to 0 \text{ as } Y \to \infty \text{ ……………..} \tag{8}$$

Where τ describes the dimensionless time, X and Y are Cartesian coordinates with dimensionless form, U, V and W are the dimensionless velocity fields, H_1 and H_3 are the dimensionless primary and secondary induced magnetic fields, θ is the temperature which is dimensionless, $G_r = \frac{gB_T(T_w - T_\infty)\upsilon}{U_\infty^{\ 3}}$ (Grashof Number), $\Delta = \frac{k}{\mu}$ (Microrotational Number), $M = \frac{1}{4\pi}\frac{H_0}{U_\infty}\sqrt{\frac{\mu_e}{\rho}}$ (Magnetic Parameter), $D_a = \frac{k' U_\infty^{\ 2}}{\upsilon^2}$ (Darcy Number), $R = \frac{2\upsilon\Omega}{U_\infty^{\ 2}}$

(Rotational Parameter), $\Lambda = \dfrac{\gamma}{j\mu}$ (Spin Gradient Viscosity), $\lambda = \dfrac{k\upsilon}{\rho j U_\infty^{\ 2}}$ (Vortex Viscosity), $P_r = \dfrac{\rho c_p \upsilon}{\kappa}$ (Prandtl Number), $E_c = \dfrac{U_\infty^{\ 2}}{c_p\left(T_w - T_\infty\right)}$ (Eckert Number), $P_m = 4\pi\sigma\upsilon\mu_e$ (Magnetic Diffusivity Parameter) and $\beta = \dfrac{Q\upsilon\left(T_w - T_\infty\right)^{p-1}}{\rho c_p U_\infty^{\ 2}}$ (Heat Absorption or Generation Parameter).

3. SHEAR AND COUPLE STRESSES, CURRENT DENSITIES AND NUSSELT NUMBER

The x directional shear stress, $\tau_x = \left\{\mu + (1-S)K\right\}\left(\dfrac{\partial u}{\partial y}\right)_{y=0}$ and the z directional shear stress, $\tau_z = \left\{\mu + (1-S)K\right\}\left(\dfrac{\partial w}{\partial y}\right)_{y=0}$ which are similar to $\left(\dfrac{\partial U}{\partial Y}\right)_{Y=0}$ and $\left(\dfrac{\partial W}{\partial Y}\right)_{Y=0}$ respectively.

Couple stress $= \dfrac{\upsilon j \rho}{\gamma}\left(\dfrac{\partial N}{\partial y}\right)_{y=0}$ which is similar to $\left(\dfrac{\partial N}{\partial Y}\right)_{Y=0}$.

Current densities along x and z directions are $J_x = \mu\left(-\dfrac{\partial H_x}{\partial y}\right)_{y=0}$ and $J_z = \mu\left(-\dfrac{\partial H_z}{\partial y}\right)_{y=0}$ which are similar to $\left(-\dfrac{\partial H_1}{\partial Y}\right)_{Y=0}$ and $\left(-\dfrac{\partial H_3}{\partial Y}\right)_{Y=0}$ respectively.

Nusselt Number $= \mu\left(-\dfrac{\partial T}{\partial y}\right)_{y=0}$ which is similar to $\left(-\dfrac{\partial \theta}{\partial Y}\right)_{Y=0}$.

4. NUMERICAL TECHNIQUE

For evaluating a free convection movement with mass transfer through a semi-infinite plate, the explicit finite difference technique has been taken by Callahan and Marner which is conditionally static [20]. On the contrast, the equivalent theory has been carried out by Soundalgekar and Ganesan through an implicit finite difference technique which is unconditionally static [21]. The major distinction between the two schemes is that the implicit scheme being unconditionally static is less extensive from the viewpoint of computer time. Anyway, these two techniques gradually employed by Callahan *et al.*, [20] and Soundalgekar *et al.*, [21] introduced the equivalent outputs. To generate the differential equations the boundary of the stream is parted into a grid of straight lines perpendicular to X and Y axes, where X -axis is accepted through the plate and Y -axis is generally perpendicular to it.

Here the plate-height $X_{\max}\left(=100\right)$ is taken i.e. X indicates from 0 to 100 and supposed $Y_{\max}\left(=40\right)$ i.e. Y indicates from 0 to 40. Now, $m\left(=125\right)$ and $n\left(=725\right)$ grid distancing in the X and Y direction accordingly as displayed in Figure 2. ΔX and ΔY are fixed mesh area along X and Y way accordingly and accepted as like, $\Delta X = 0.8\left(0 \le X \le 100\right)$ and $\Delta Y = 0.055$ (approx.) $\left(0 \le Y \le 40\right)$ with the shorter time-step, $\Delta\tau = 0.0005$.

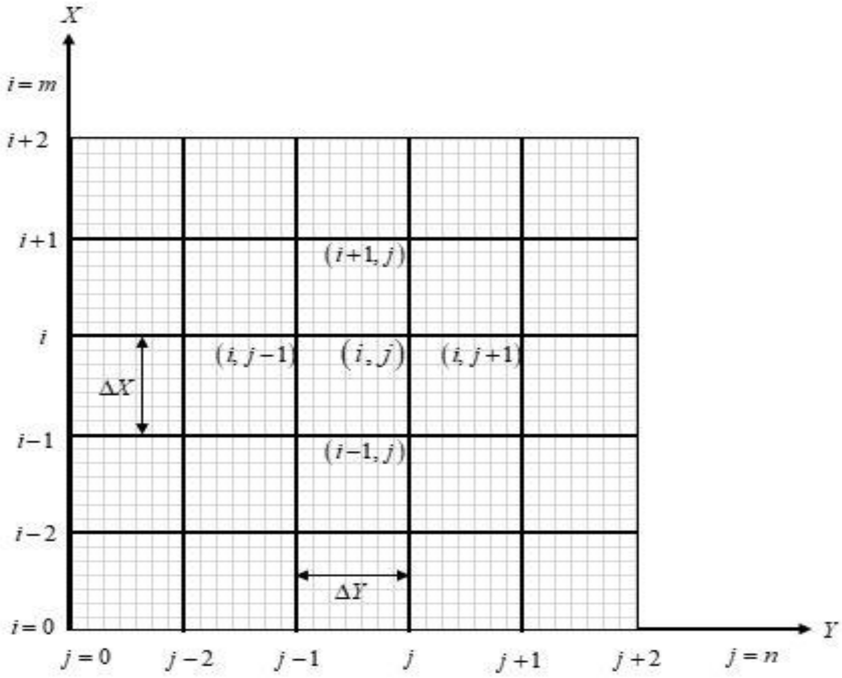

Figure 2: EFDM system grid

Let U', W', N', H_1', H_3' and θ' explain the values of U, W, N, H_1, H_3 and θ are the last of a time-step in some respects. Conducting the explicit finite difference theory, the scheme of partial differential equations (9)-(15) is found by an inferential group of finite difference equations;

$$\frac{U_{i,j}-U_{i-1,j}}{\Delta X}+\frac{V_{i,j+1}-V_{i,j}}{\Delta Y}=0 \tag{9}$$

$$\frac{U'_{i,j}-U_{i,j}}{\Delta\tau}+U_{i,j}\frac{U_{i,j}-U_{i-1,j}}{\Delta X}+V_{i,j}\frac{U_{i,j+1}-U_{i,j}}{\Delta Y}=G_r\theta_{i,j} \tag{10}$$

$$+(1+\Delta)\frac{U_{i,j+1}-2U_{i,j}+U_{i,j-1}}{(\Delta Y)^2}+\Delta\frac{N_{i,j+1}-N_{i,j}}{\Delta Y}+M\frac{H_{1i,j+1}-H_{1i,j}}{\Delta Y}-\frac{U_{i,j}}{D_a}-RW_{i,j}$$

$$\frac{W'_{i,j}-W_{i,j}}{\Delta\tau}+U_{i,j}\frac{W_{i,j}-W_{i-1,j}}{\Delta X}+V_{i,j}\frac{W_{i,j+1}-W_{i,j}}{\Delta Y} \tag{11}$$

$$=(1+\Delta)\frac{W_{i,j+1}-2W_{i,j}+W_{i,j-1}}{(\Delta Y)^2}+M\frac{H_{3i,j+1}-H_{3i,j}}{\Delta Y}-\frac{W_{i,j}}{D_a}+RU_{i,j}$$

$$\frac{N'_{i,j}-N_{i,j}}{\Delta\tau}+U_{i,j}\frac{N_{i,j}-N_{i-1,j}}{\Delta X}+V_{i,j}\frac{N_{i,j+1}-N_{i,j}}{\Delta Y} \tag{12}$$

$$=\Lambda\frac{N_{i,j+1}-2N_{i,j}+N_{i,j-1}}{(\Delta Y)^2}-\lambda\frac{U_{i,j+1}-U_{i,j}}{\Delta Y}-2\lambda N_{i,j}$$

$$\frac{H_1{}'_{i,j}-H_{1i,j}}{\Delta\tau}+V_{i,j}\frac{H_{1i,j+1}-H_{1i,j}}{\Delta Y}=\frac{1}{P_m}\frac{H_{1i,j+1}-2H_{1i,j}+H_{1i,j-1}}{(\Delta Y)^2}+H_{1i,j}\frac{U_{i,j}-U_{i-1,j}}{\Delta X} \tag{13}$$

$$+M\frac{U_{i,j+1}-U_{i,j}}{\Delta Y}-\frac{\beta_e}{P_m}\frac{H_{3i,j+1}-2H_{3i,j}+H_{3i,j-1}}{(\Delta Y)^2}$$

$$\frac{H_3{'}_{i,j}-H_{3i,j}}{\Delta\tau}+V_{i,j}\frac{H_{3i,j+1}-H_{3i,j}}{\Delta Y}=\frac{1}{P_m}\frac{H_{3i,j+1}-2H_{3i,j}+H_{3i,j-1}}{(\Delta Y)^2}+H_{1i,j}\frac{W_{i,j}-W_{i-1,j}}{\Delta X}$$
$$+M\frac{W_{i,j+1}-W_{i,j}}{\Delta Y}+\frac{\beta_e}{P_m}\frac{H_{1i,j+1}-2H_{1i,j}+H_{1i,j-1}}{(\Delta Y)^2} \tag{14}$$

$$\frac{\theta'_{i,j}-\theta_{i,j}}{\Delta\tau}+U_{i,j}\frac{\theta_{i,j}-\theta_{i-1,j}}{\Delta X}+V_{i,j}\frac{\theta_{i,j+1}-\theta_{i,j}}{\Delta Y}=\frac{1}{P_r}\frac{\theta_{i,j+1}-2\theta_{i,j}+\theta_{i,j-1}}{(\Delta Y)^2}$$
$$+\frac{E_c}{P_m}\left\{\left(\frac{H_{3i,j+1}-H_{3i,j}}{\Delta Y}\right)^2+\left(\frac{H_{1i,j+1}-H_{1i,j}}{\Delta Y}\right)^2\right\}$$
$$+E_c\left\{\left(\frac{U_{i,j+1}-U_{i,j}}{\Delta Y}\right)^2+\left(\frac{W_{i,j+1}-W_{i,j}}{\Delta Y}\right)^2\right\}+\beta\,\theta_{i,j}{}^{p} \tag{15}$$

and the boundary condition creates,

$$U^n_{i,0}=1, V^n_{i,0}=0, W^n_{i,0}=0, N^n_{i,0}=-S\frac{\partial U^n_{i,0}}{\partial Y}, H^{\;n}_{1i,0}=1(\text{say}), H^{\;n}_{3i,0}=0, \theta^n_{i,0}=1 \text{ at } Y=0$$
$$U^n_{i,L}=0, V^n_{i,L}=0, W^n_{i,L}=0, N^n_{i,L}=0, H^{\;n}_{1i,L}=0, H^{\;n}_{3i,L}=0, \theta^n_{i,L}\to 0 \text{ as } Y=L\to\infty$$

Above the subscript i and j determines the grid spots with X and Y coordinates serially and the superscript n determines a standard of time, $\tau=n\Delta\tau$ where $n=0,1,2,\ldots$. The numerical solutions of the shear and couple stress, current densities, and Nusselt number are established by the Three-Point law.

The stability agreements of the system are described below as:

$$\frac{\Delta\tau}{2D_a}+2(1+\Delta)\frac{\Delta\tau}{(\Delta Y)^2}+U\frac{\Delta\tau}{\Delta X}+|-V|\frac{\Delta\tau}{\Delta Y}\le 1,\ \Delta\tau\lambda+U\frac{\Delta\tau}{\Delta X}+|-V|\frac{\Delta\tau}{\Delta Y}+2\Lambda\frac{\Delta\tau}{(\Delta Y)^2}\le 1,$$
$$|-V|\frac{\Delta\tau}{\Delta Y}+\frac{2}{P_m}\frac{\Delta\tau}{(\Delta Y)^2}\le 1 \text{and} U\frac{\Delta\tau}{\Delta X}+|-V|\frac{\Delta\tau}{\Delta Y}+\frac{2}{P_r}\frac{\Delta\tau}{(\Delta Y)^2}-\Delta\tau\beta\theta^{p-1}\le 1.$$

5. RESULTS AND DISCUSSION

This section discusses the influence of non-dimensional parameters on the physical insight of flow characteristics of the ECF fluid and presents in Figs. 3-8. In particular, the influence of spin gradient viscosity (Λ), vortex viscosity (λ), magnetic diffusivity number (P_m), and heat absorption parameter (β) are discussed, whereas the other non-dimensional parameters are not addressed for the sake of brevity. The flow characteristics are discussed in terms of primary and secondary velocities, wall shear stresses along x and z directions, angular velocity, couple stress, primary and secondary induced magnetic fields, current density along x and z directions, temperature profile, and Nusselt number. The numerical computation has been carried out up to the dimensionless time $\tau=40$ to secure the steady-state situation. It was observed that all the flow characteristics show identical curves at each iteration for $\tau\ge 30$. Therefore, the results at $\tau=30$ can be considered steady-state outcomes, and all the results are presented at their steady state.

Primary and secondary velocities:

Figure 3 shows the outcomes of Λ, λ, P_m ,and β on the primary (top) and secondary (bottom) velocity profiles. It can be seen that the primary velocity decreases with rising λ whereas rises with Λ, see Fig. 3(a). Furthermore, Fig. 3(b) shows that the primary velocity reduces when P_m rises while it is increases with rising β. Secondary velocity rises for the rising data of λ and reduce for the rising values of Λ, see Fig. 3(a). Furthermore, Fig. 3(b) shows that the secondary velocity reduce for the rising data of P_m, and β.

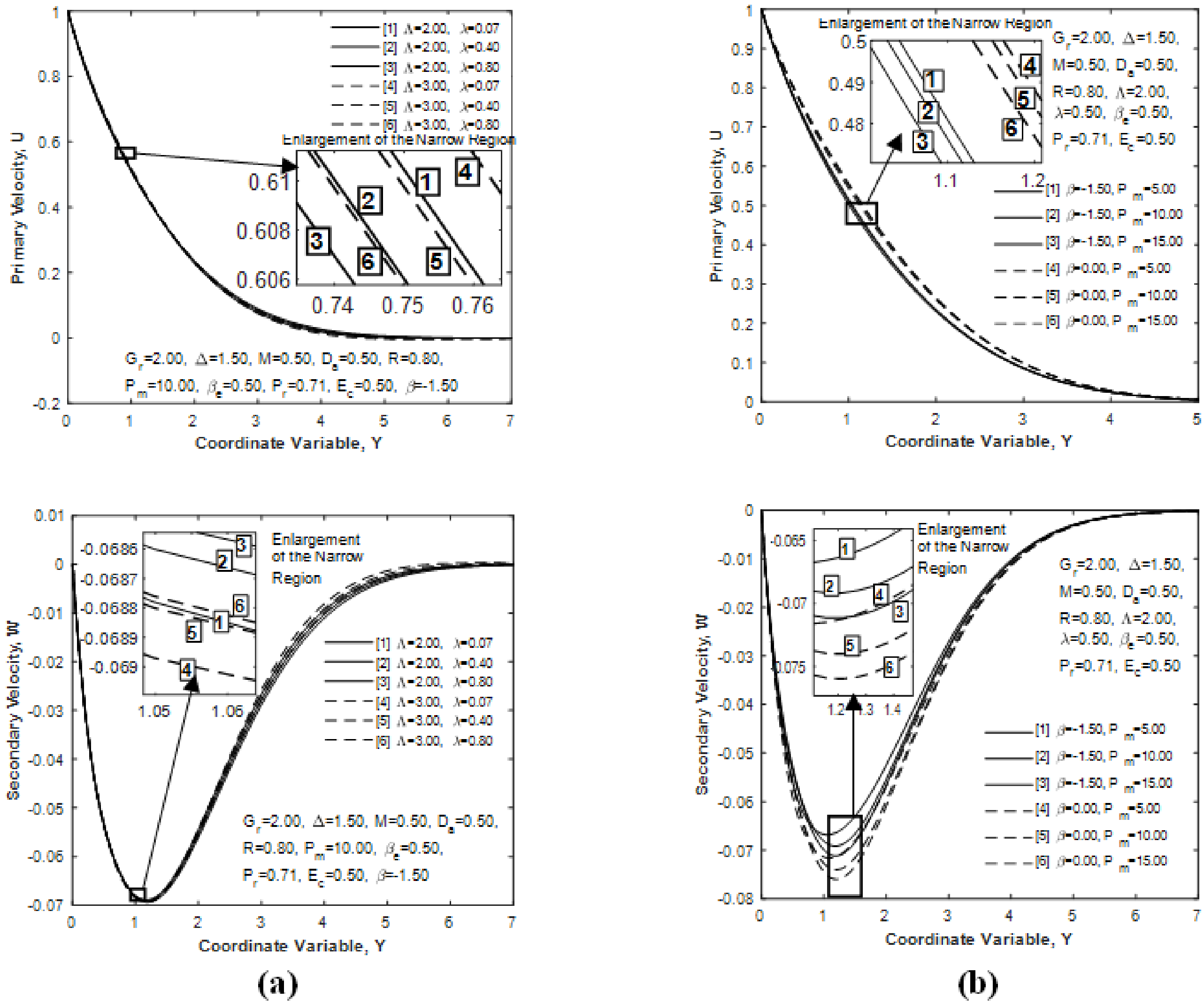

Figure-3: Primary (top) and secondary (bottom) velocity distributions as a function of dimensionless parameters (a) Λ and λ; (b) P_m and β

Wall shear stresses along x and z directions

Figure 4 shows the effect of Λ, λ, P_m ,and β on the wall shear stresses along x (top) and z (bottom) directions. It can be seen that wall shear stress along x direction reduce for the rising data of λ and rise for the increasing data of Λ, see Fig. 4(a). Furthermore, Fig. 4(b) shows that shear stress along x direction reduce for the rising values of P_m and increase for the rising data of β. It can be seen that the shear stress along with z -direction increase for the rising data of λ and reduce for the rising values of Λ, see Fig. 4(a). Furthermore, Fig. 4(b) shows that the shear stress along z -direction reduce for the rising data of P_m and β.

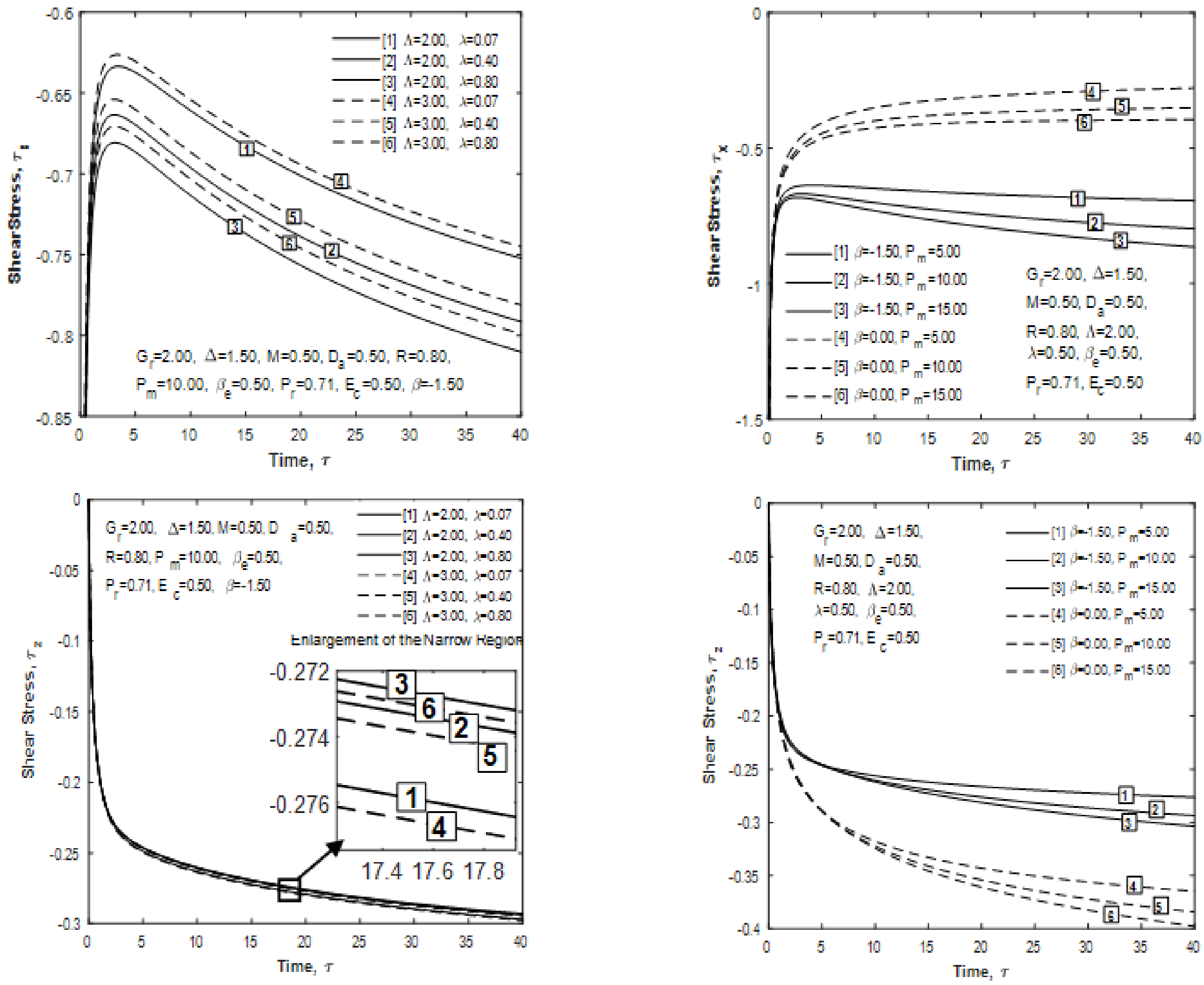

(a) **(b)**

Figure-4: Wall shear stresses along x (top) and z (bottom) directions as a function of dimensionless parameters (a) Λ and λ; (b) P_m and β

Angular velocity and couple stress

Figure 5 shows the effect of Λ, λ, P_m, and β on the angular velocity (top) and couple stress (bottom). It can be seen that angular velocity increases for the rising values of λ and reduces for the rising data of Λ, see Fig. 5(a). Furthermore, Fig. 5(b) shows that angular velocity rises for the rising values of P_m and reduces for the rising data of β. It can be seen that couple stress reduces for the rising data of λ and increases for the rising data of Λ, see Fig. 5(a). Furthermore, Fig. 5(b) shows that couple Stress reduces for the rising data of P_m and rises for the rising data of β.

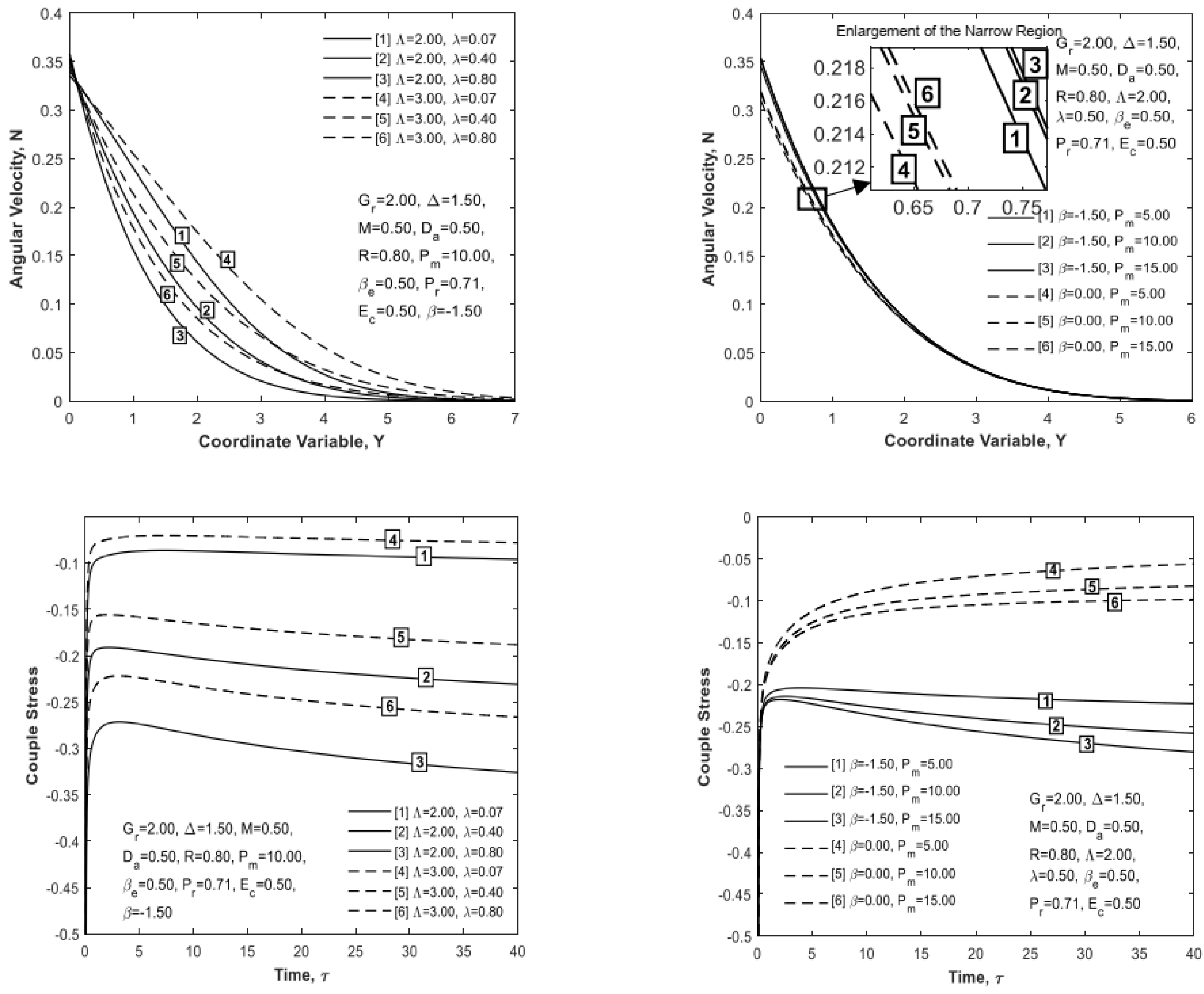

(a) **(b)**

Figure-5: Angular velocity (top) and couple stress (bottom) as a function of dimensionless parameters (a) Λ and λ; (b) P_m and β

Primary and secondary induced magnetic fields

Figure 6 shows the effect of Λ, λ, P_m ,and β on the primary (top) and secondary (bottom) induced magnetic field. It can be seen that primary induced magnetic field reduces for the rising values of λ and rises for the rising data of Λ, see Fig. 6(a). Furthermore, Fig. 6(b) shows that primary induced magnetic field reduces for the rising data of P_m and rises for the rising data of β .Secondary induced magnetic field reduces for the rising data of λ and rises for the rising values of Λ , see Fig. 6(a). Furthermore, Fig. 6(b) shows that secondary induced magnetic field decreases for the rising values of P_m and increases for the rising values of β .

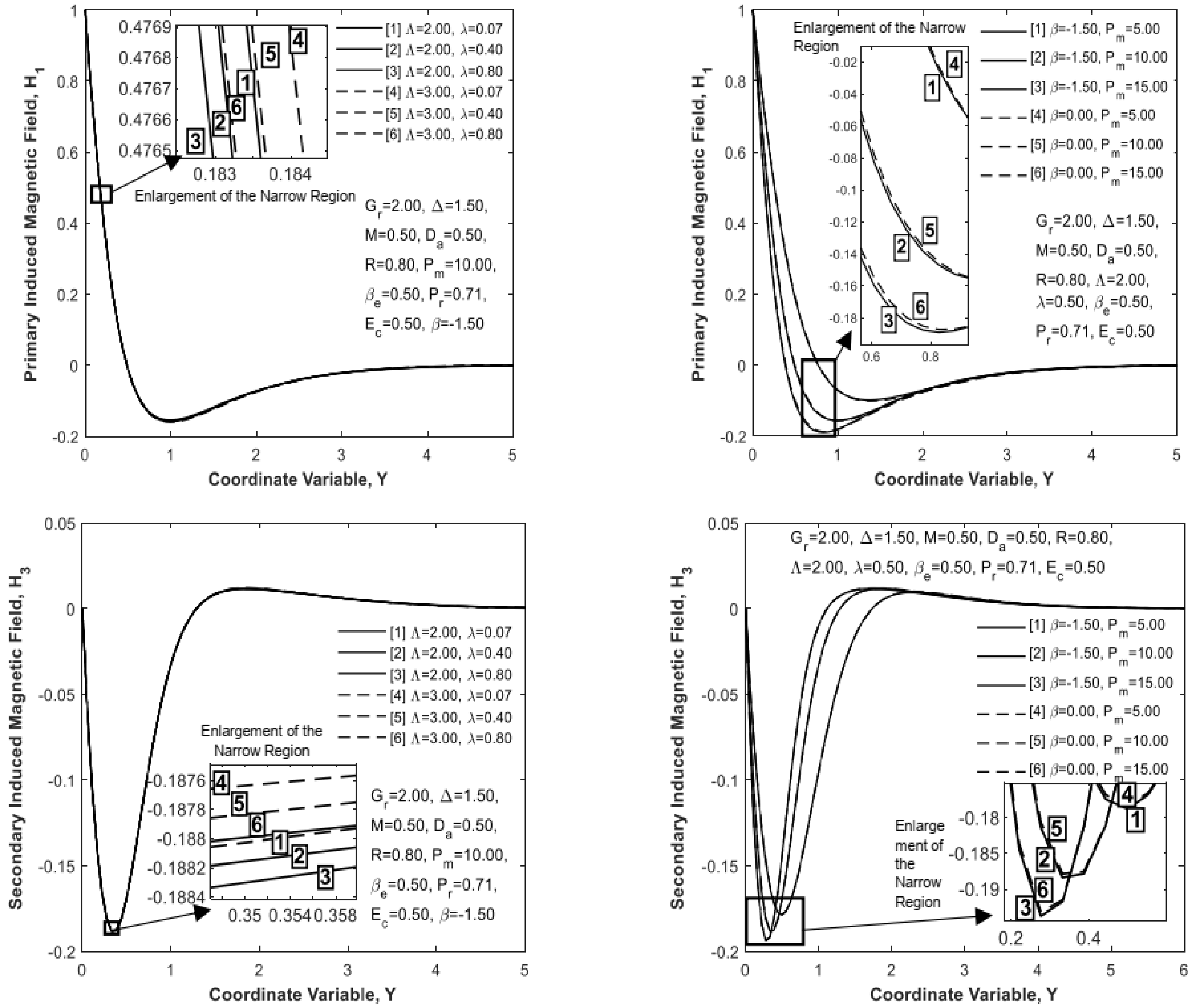

(a) **(b)**

Figure-6: Primary (top) and secondary (bottom) induced magnetic field as a function of dimensionless parameters (a) Λ and λ; (b) P_m and β

Current density along x and z directions:

Figure 7 shows the effect of Λ, λ, P_m,and β on the current density along x (top) and z (bottom) directions. It can be seen that current density along with x-direction rises for the rising data of λ and reduces for the rising data of Λ, see Fig. 7(a). Furthermore, Fig. 7(b) shows that current density along with x-direction increases for the rising data of P_m and reduces for the rising data of β.It can be seen that current density along with z-direction rises for the rising values of λ and reduces for the rising data of Λ, see Fig. 7(a). Furthermore, Fig. 7(b) shows that current density along with z-direction rises for the rising data of P_m and reduces for the rising data of β.

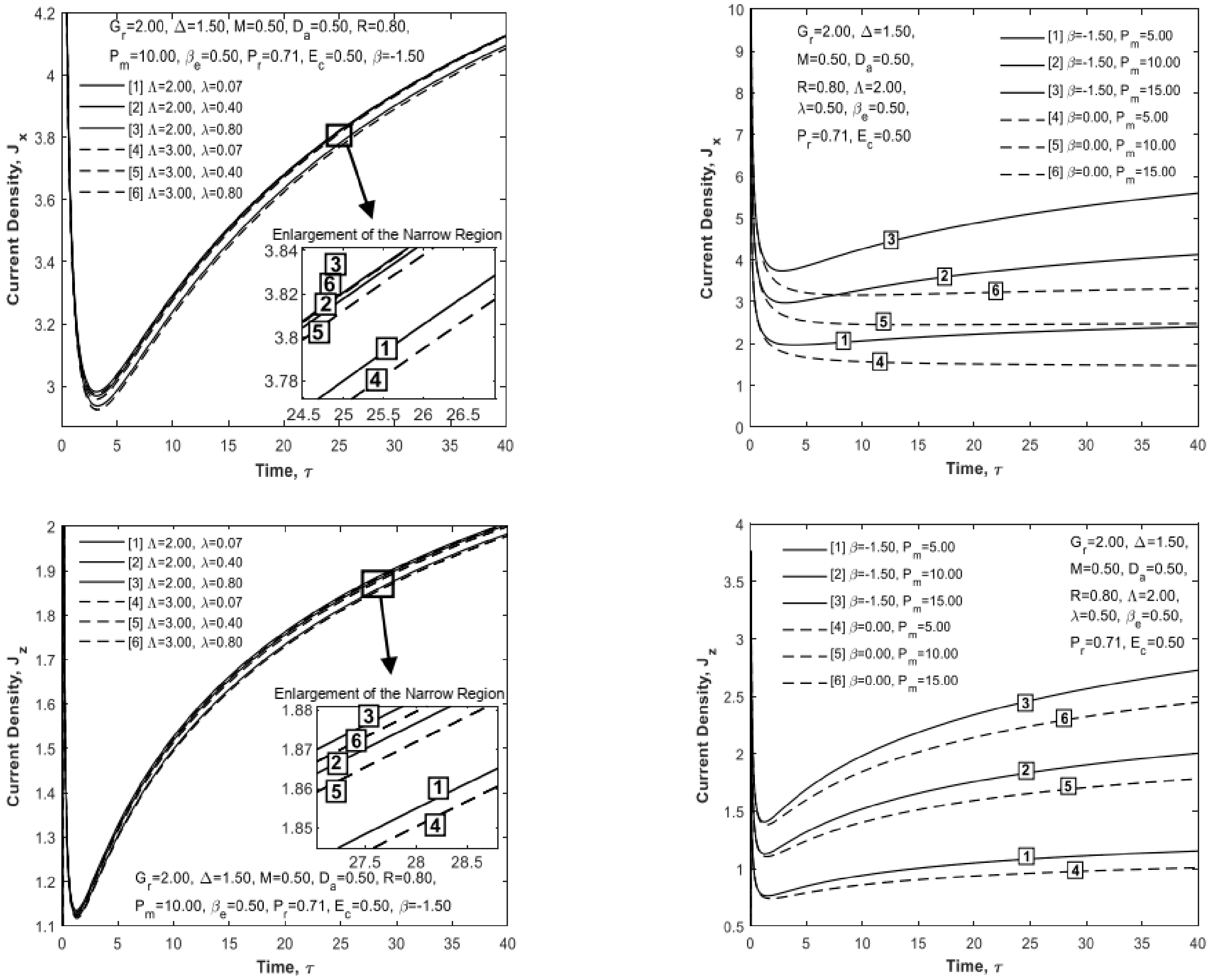

(a) **(b)**

Figure-7: Current density along x (top) and z (bottom) directions as a function of dimensionless parameters (a) Λ and λ; (b) P_m and β

Temperature profile and Nusselt number

Figure 8 shows the effect of Λ, λ, P_m, and β on the temperature profile (top) and Nusselt number (bottom). It can be seen that temperature rises for the increasing values of λ and reduces for the rising data of Λ, see Fig. 8(a). Furthermore, Fig. 8(b) shows that temperature reduces for the rising data of P_m and rises for the rising data of β. Nusselt number reduces for the rising data of λ and rises for the rising data of Λ, see Fig. 8(a). Furthermore, Fig. 8(b) shows that Nusselt number on rises for the rising data of P_m and decreases for the rising data of β.

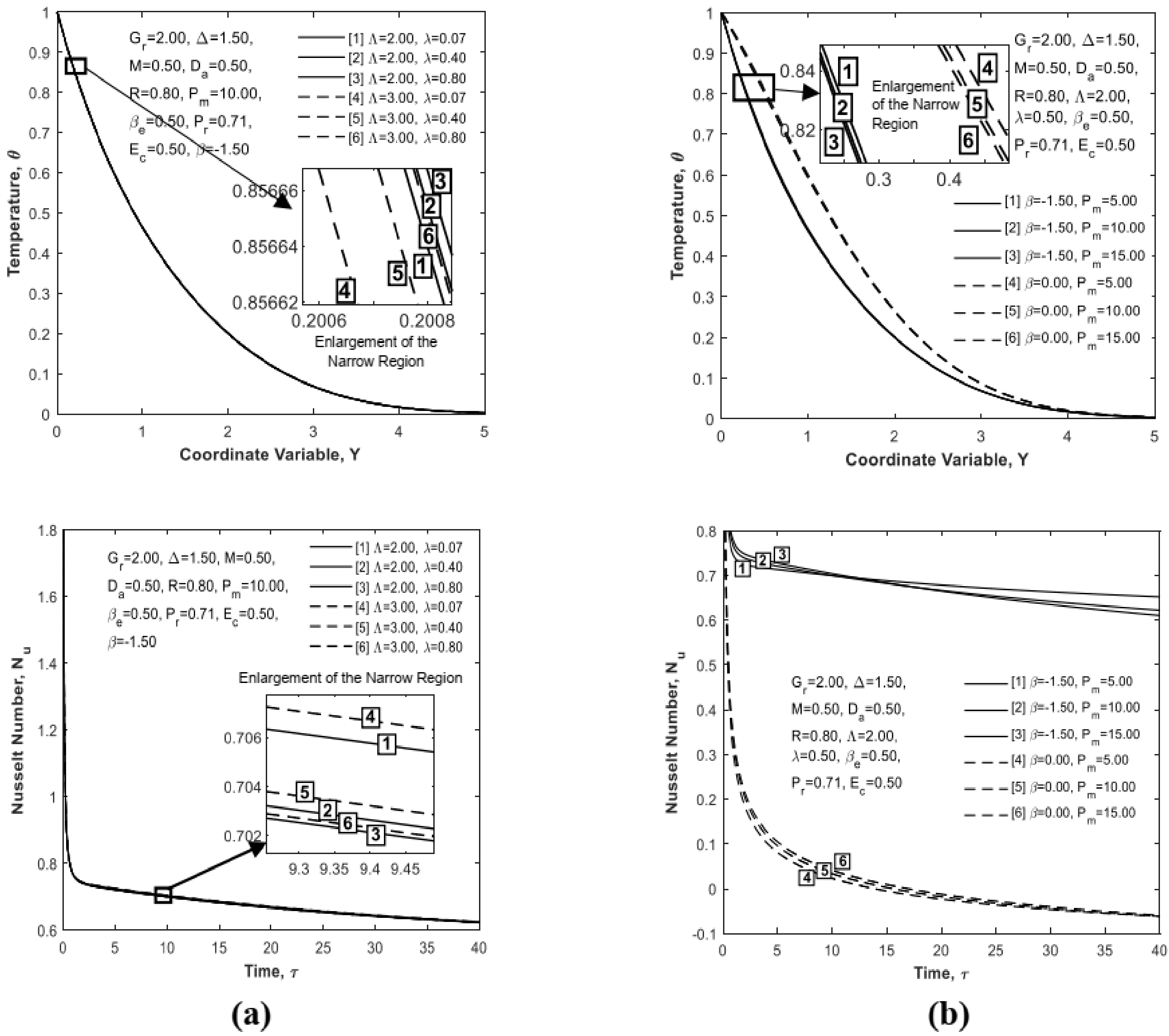

Figure-8: Temperature profile (top) and Nusselt number (bottom) as a function of dimensionless parameters (a) Λ and λ; (b) P_m and β

6. CONCLUSIONS

This manuscript has over seen the outcome of transverse magnetic field regarding Hall current with a porous perpendicular plate. EFDM investigations are established for different data of the dimensionless parameters. Several significant outcomes of this lesson are shown below:

1. The primary velocity and the x -directional shear stress rise with the incrementing of Λ, β and reduce with the increasing of λ, P_m.
2. The secondary velocity and the z -directional shear stress rise with the incrementing of λ and reduce with the incrementing of Λ, P_m, β.
3. The angular velocity rises with the incrementing of λ, P_m and reduces with the incrementing of Λ, β. The couple stress rises with the incrementing of Λ, β and reduces with the incrementing of λ, P_m.
4. The primary induced magnetic field increases with the incrementing of Λ, β and reduces with the incrementing of λ, P_m. The x -directional current density increases with the incrementing of λ, P_m and reduces with the incrementing of Λ, β.
5. The secondary induced magnetic field rises with the incrementing of Λ, β and reduces

with the incrementing of λ , P_m .The z -direction current density rises with the incrementing of λ, P_m and reduces with the incrementing of Λ, β.

6. The temperature rises with the incrementing of λ, β and reduces with the incrementing of Λ , P_m .The Nusselt number rises with the incrementing of Λ, P_m and reduces with the incrementing of λ, β.

Based on this work, a more general model for intravascular extracellular fluid and interstitial extracellular fluid can be developed for future researches. Therefore, the fluid movement tendency and temperature distribution effects in the human and animal bodies can be described more visibly and accurately.

REFERENCES

1. Ezzat, M. (2004). Free convection effects on extracellular fluid in the presence of a transverse magnetic field. *Applied Mathematics and Computation*, 151(2), 455-482. https://doi.org/10.1016/S0096-3003(03)00354-0
2. Hodgkin, A. L., Huxley, A. F., & Eccles, S. J. (1959). The influence of potassium and chloride ions on the membrane potential of single muscle fibers. *J Physiol*, 148, 127. https://doi.org/10.1113/jphysiol.1959.sp006278
3. Eringen, A. C. (1966). Theory of micropolar fluids. *Journal of Mathematics and Mechanics*, 6(1), 1-18. https://www.jstor.org/stable/24901466
4. Kline, K. A., Alien, S. J. (1969). Concentration effects in oscillatory blood flow. *Biorheology*, 6(2), 99. https://doi.org/10.3233/bir-1969-6204
5. Ariman, T. (1971). On the analysis of blood flow. *Journal of Biomechanics*, 4, 185-192. https://doi.org/10.1016/0021-9290(71)90003-0
6. Ariman, T., Turk, M. A., & Sylvester, N. D. (1973). Microcontinuum fluid mechanics-a review. *International Journal of Engineering Science*, 11(8), 905-930. http://dx.doi.org/10.1016/0020-7225(73)90038-4
7. Eringen, A. C. (1972). Theory of thermomicro fluids. *Journal of Mathematical Analysis and Applications*, 38(2), 480-496. https://doi.org/10.1016/0022-247X(72)90106-0
8. Ezzat, M., Othman, M., & Helmy, K. (1999). A problem of a micropolar magneto-hydrodynamic boundary-layer flow. *Canadian Journal of Physics*, 77, 813-827. https://doi.org/10.1139/p99-061
9. Ezzat, M. (2001). Free convection effects on perfectly conducting fluid. *International Journal of Engineering Science*, 39(7), 799-819. https://doi.org/10.1016/S0020-7225(00)00059-8
10. Bhargava, R., Kumar, L., & Takhar, H. S. (2003). Numerical solution of free convection MHD micropolar fluid flow between two parallel porous vertical plates. *International Journal of Engineering Science*, 41, 123-136. https://doi.org/10.1016/S0020-7225(02)00157-X
11. Mohammadein, A. A., & Gorla, R. S. R. (1996). Effects of transverse magnetic field on mixed convection in a micropolar fluid on a horizontal plate with vectored mass transfer. *Actamechanica*, 118(1-4), 1-12. https://doi.org/10.1007/BF01410503
12. Postelnicu, A. (2004). Influence of a magnetic field on heat and mass transfer by natural convection from vertical surfaces in porous media considering Soret and Dufour effects. *International Journal of Heat and Mass Transfer*, 47(6-7), 1467-1472. https://doi.org/10.1016/j.ijheatmasstransfer.2003.09.017
13. Peddiesen, J., & McNItt, R. P. (1970). Boundary layer theory for a micropolar fluid. *Recent Advanced Engineering and Science*, 5, 405.
14. Ram, P. C. (1988). Unsteady MHD free-convective flow through a porous medium with Hall currents. *Astrophysics and Space Science*, 149, 171-174. https://doi.org/10.1007/BF00640477
15. Garg, B. P. (2012). Combined effects of thermal radiations and Hall current on moving vertical porous plate in a rotating system with variable temperature. *International Journal of Pure and Applied Mathematics*, 81(2), 335-345.
16. Kafoussias, N. G., & Williams, E. W. (1995). Thermal-dissusion and diffusion-thermo effects on mixed free-forced convective and mass transfer boundary layer flow with temperature dependent viscosity. *International Journal of Engineering Science*, 33(9), 1369-1384.
17. Shateyi, S., Motsa, S. S., & Sibanda, P. (2010). The effects of thermal radiation, hall currents, soret, and dufour on MHD flow by mixed convection over a vertical surface in porous media. *Mathematical Problems in Engineering*, *2010*.
18. Ahmed, T., & Alam, M. M. (2013). Finite difference solution of MHD mixed convection flow with heat generation and chemical reaction. *Procedia Engineering*, *56*, 149-156.
19. Takhar, H. S., Chamkha, A. J., & Nath, G. (2002). MHD flow over a moving plate in a rotating fluid with magnetic field, Hall currents and free stream velocity. *International Journal of Engineering Science*, *40*(13), 1511-1527.
20. Callahan, G. D., & Marner, W. J. (1976). Transient free convection with mass transfer on an isothermal vertical flat plate. *International Journal of Heat and Mass Transfer*, *19*(2), 165-174.
21. Soundalgekar, V. M., & Ganesan, P. (1980). Transient free convective flow past a semi-infinite vertical plate with mass transfer. *Journal of Energy Heat and Mass Transfer*, *2*(1), 83-91.